PAPER

Alignment method based on direct establishment of global world coordinate system for 3D laser vibrometry

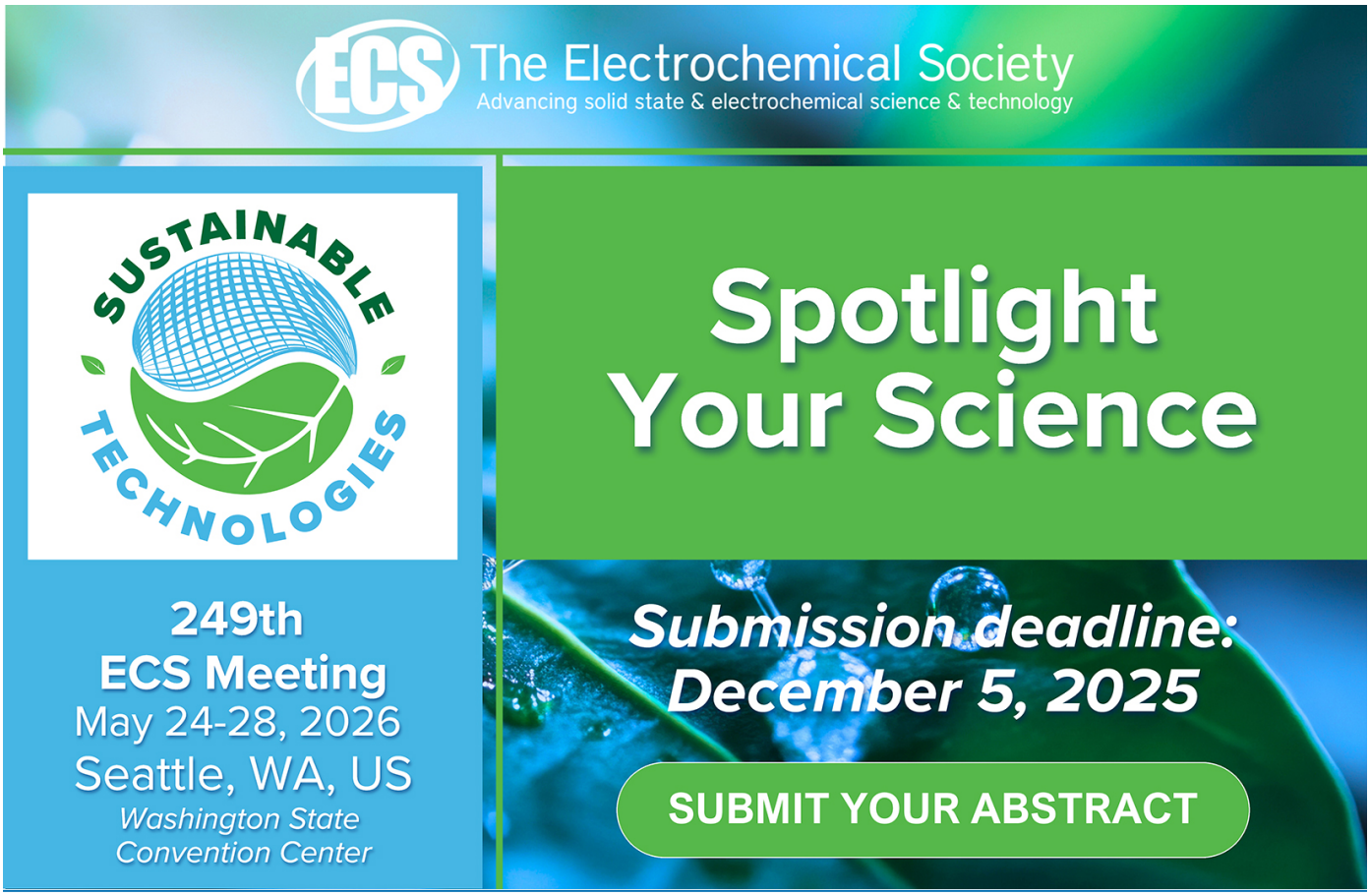

IOP Publishing Measurement Science and Technology
Meas. Sci. Technol. **36** (2025) 085904 (9pp) https://doi.org/10.1088/1361-6501/adf4fd

Alignment method based on direct establishment of global world coordinate system for 3D laser vibrometry

Huang Xinjing[1], Lai Ruqiang[1], Zhang Zhipeng[1], Zhang Tao[2], Li Zhengzhe[1], Li Jian[1] and Ma Jinyu[1,*]

[1] State Key Laboratory of Precision Measurement Technology and Instruments, Tianjin University, Tianjin, People's Republic of China
[2] Tianjin Institute of Metrology Supervision and Testing, Tianjin, People's Republic of China

E-mail: jinyu.ma@tju.edu.cn

Received 2 May 2025, revised 16 June 2025
Accepted for publication 28 July 2025
Published 29 August 2025

Abstract

Three-dimensional (3D) full-field scanning laser Doppler vibrometry represents one of the most significant non-contact vibration measurement technologies currently available. Among its core components, 3D alignment and laser vibrometry constitute the two most critical technical elements. 3D alignment obtains the rotation matrices from the local probe coordinate system (PCS) to the global world coordinate system (WCS), thereby mapping non-orthogonal vibration components measured along three laser beam directions by three probes into the orthogonal WCS. However, existing alignment methods demonstrate significant dependence on calibration plates or additional measurement equipment, while exhibiting limited adaptability to complex curved structures, thus constraining their engineering applications. To address this issue, this paper proposes a 3D alignment algorithm based on the developed mathematical model of 2D rotating mirror outgoing light rays that directly establishes the global WCS on the measured object surface. This method utilizes the geometric constraint relationships between multiple laser beam's direction vectors and the WCS when multiple probes illuminate the same point, thereby solving for the transformation matrix from the PCS to the WCS. This approach eliminates the dependence on calibration plates or feature points that is characteristic of conventional methods. Experimental results demonstrate that the method achieves maximum average relative errors of 2.85% and 6.53% in planar and curved surface alignment scenarios, respectively, while simultaneously enabling 3D full-field laser scanning. Compared to existing technologies, the proposed method exhibits significant advantages in terms of scenario adaptability and engineering practicality.

Keywords: laser Doppler vibrometer, mirror model, 3D alignment

* Author to whom any correspondence should be addressed.

1. Introduction

Laser Doppler vibrometer (LDV) technology represents a high-precision, non-contact vibration measurement technique based on the optical Doppler effect. The LDV system emits a detection laser beam toward the surface of the measured object and receives optical signals with frequency shifts in the scattered light caused by target vibrations. These signals are then processed through interference demodulation methods to reconstruct vibration velocity information. The technology exhibits significant advantages including non-contact operation, wide bandwidth, and high resolution, which has led to its widespread application in modal testing analysis, structural health monitoring, ultrasonic flaw detection, and related fields [1–3].

LDVs can be classified into three categories: one-dimensional (1D), three-dimensional (3D), and 3D full-field scanning (FFS) systems. 1D LDVs only capture vibration components along the laser beam direction, with measurement accuracy significantly affected by the angle between the laser and vibration directions, and are unable to characterize complex 3D vibration modes [4, 5]. Additionally, single-probe movement methods on mobile platforms face severe speckle noise challenges that can significantly degrade signal quality [6]. 3D LDVs operate through the collaborative functioning of three 1D LDVs [7], requiring focused laser convergence at a single point and relying on coordinate transformation to achieve 3D vibration measurement at single point. However, equipment calibration must be repeated when switching between different measurement points. In contrast, 3D LDV FFS utilizes galvanometer deflection to control three laser beams to automatically track arbitrary measurement points on the target surface. This approach enables high-precision 3D vibration measurements across the entire view field without requiring equipment position adjustments, demonstrating significant advantages in efficiency and adaptability to complex scenarios [8].

Current 3D vibration measurement techniques are primarily categorized into two approaches: single-probe movement methods and multi-probe collaborative methods. Single-probe movement methods are implemented through adjusting the position and orientation of an individual 1D LDV using scanners [9, 10], robotic arms [11], or image registration techniques [12]. Although these methods offer cost advantages, they cannot synchronously acquire instantaneous 3D vibration data and introduce mechanical errors, so they are only competent to steady-state vibration measurement. Multi-probe collaborative methods can be achieved through either 3D LDV or 3D FFS LDV systems. 3D vibration measurement using 3D LDV requires three 1D LDVs to synchronously measure 3D vibration at a single point, making this method suitable for single-point vibration measurement applications [13–15]. For scanning applications, multiple calibrations of laser beam convergence are typically required [16]. Although 3D vibration measurement techniques based on 3D FFS LDV enable scanning capabilities, they predominantly require calibration plates, reference objects [17, 18] or feature points on the measured object itself [19] to provide world coordinates for alignment points, which constrains their practical applications.

LDV measurement probes can only measure vibration velocity along their laser beam directions. The three probes of a 3D LDV system are typically arranged arbitrarily in the field, resulting in three non-orthogonal detection laser beams. To achieve orthogonal decomposition of 3D vibration components in the world coordinate system (WCS), the known laser beam measurement directions in each probe coordinate system (PCS) must be mapped to unit vectors in the WCS using transformation matrices from each PCS to the WCS. The precise determination of these transformation matrices constitutes 3D alignment, which represents one of the core components of 3D vibration measurement.

Nevertheless, existing methods for calculating transformation matrices exhibit certain limitations that hinder their application in 3D alignment of 3D FFS LDV. Zeng *et al* [20] proposed a rotation matrix calculation method based on least squares, which requires more than four alignment points and demonstrates sensitivity to initial iteration values, frequently generating matrices with opposite signs. Martarelli *et al* [21] investigated the influence of alignment point quantity and distribution on measurement accuracy; however, their method relies on theodolite calibration to establish global coordinates. Xu and Miles [22] introduced an inverse solution method. This method utilizes four reference points with known coordinates in both global and PCSs. These reference points must be distributed across different planes, thereby limiting its application to curved surfaces or other complex structural analyses. Furthermore, this method does not guarantee orthogonality of the resulting matrix, which is inconsistent with physical reality, limiting its application to scenarios where orthogonal matrices can be inherently obtained. Chen and Zhu [17] improved these methods by employing singular value decomposition to directly calculate orthogonal transformation matrices through multi-target point coordinates, thereby overcoming structural constraints and ensuring analytical precision of 3D velocity vectors. Despite these advances, all aforementioned methods require additional equipment such as calibration plates or theodolites to obtain the coordinates of alignment points in the WCS. Moreover, existing evaluation approaches only calculate errors based on limited test points, failing to comprehensively assess algorithm performance across the entire scanning space or reflect systematic errors from laser beam directional variations.

Addressing the limitations of traditional 3D alignment methods that depend on external calibration tools and exhibit insufficient scenario adaptability, this study presents an innovative 3D alignment method that directly establishes the WCS on the surface of the measured object. Meanwhile, we propose a spherical coordinate-based double integral error evaluation method that can more comprehensively assess algorithm performance and accurately reflect the impact of laser beam directional variations on measurement accuracy. This paper

analyzes the requirements and principles of 3D alignment, establishes a mathematical model for outgoing light rays from two-dimensional galvanometer mirrors, and combines this with the established WCS to determine the rotation matrices required for 3D alignment. Finally, flat plates and pipes are selected as two typical measurement objects to experimentally validate the accuracy of the proposed 3D alignment method, demonstrating the method's versatility in both planar and curved surface applications for industrial measurement environments.

2. Method

2.1. Requirements and principles of 3D alignment

Compared to 1D laser vibrometers, the fundamental advantage of 3D laser vibrometers lies in their ability to precisely analyze 3D vibration vectors of the target. The key to this capability resides in determining the rotation matrices between the PCS and the WCS, thereby establishing positional relationships among multiple probes. This process transforms velocity vectors from each PCS into the WCS, ultimately calculating the 3D velocity $\mathbf{V}_\mathrm{w}$ at the target point.

Let $\mathbf{e}$ denote the unit direction vector of the laser beam emitted by the probe in the PCS and $\mathbf{R}$ represent the rotation matrix between the PCS and the WCS, then the unit direction vector of the laser beam in the WCS, $\mathbf{e}'$, can be expressed as:

$$\mathbf{e}' = \mathbf{R}\mathbf{e}. \tag{1}$$

In vibrometers, the scalar velocity measured by the probe equals the projection of the target point velocity onto the laser beam direction in the WCS. Therefore, for the ith probe:

$$v_i = \mathbf{e}_\mathrm{i}'^{\mathrm{T}} \cdot \mathbf{V}_\mathrm{w}. \tag{2}$$

In the equation, $\mathbf{e}_\mathrm{i}'$ represents the unit direction vector of a laser beam emitted by a probe in the WCS; v_i denotes the scalar vibration velocity measured by the probe along its beam direction. Based on the rotation matrix between the PCS and the WCS, the 3D velocity $\mathbf{V}_\mathrm{w}$ in the WCS is calculated as follows:

$$\mathbf{V}_\mathrm{w} = \begin{bmatrix} \mathbf{e}_1'^{\mathrm{T}} \\ \mathbf{e}_2'^{\mathrm{T}} \\ \mathbf{e}_3'^{\mathrm{T}} \end{bmatrix}^{-1} \cdot \begin{bmatrix} v_1 \\ v_2 \\ v_3 \end{bmatrix}. \tag{3}$$

Based on the above analysis, the key to achieving 3D FFS for 3D LDV lies in accurately determining the rotation matrices. To address this issue, a 3D scanning laser control system was designed as illustrated in figure 1. The system comprises three identical scanning probes, a scanning control system, and a camera. Within this system, the camera provides feedback on of laser output positions from the probes to the host computer. The scanning probes, composed of laser rangefinders and 2D rotating mirrors, enable spatial angle control of outgoing laser beams and distance measurement of laser

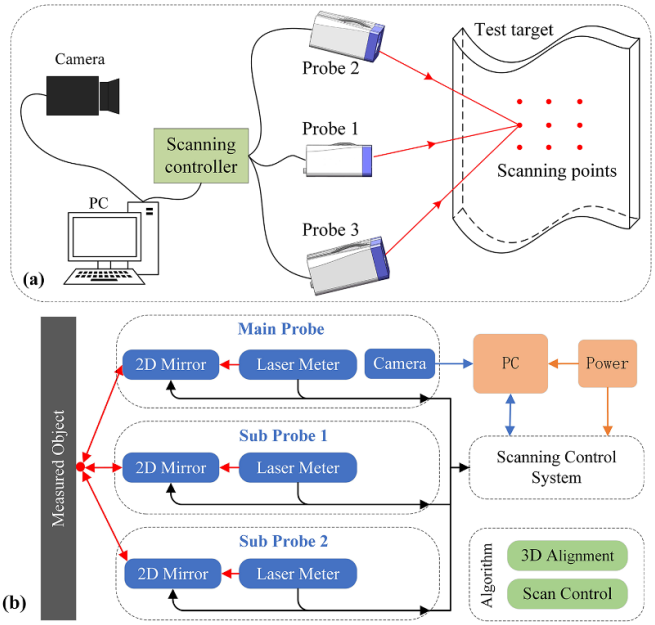

Figure 1. System block diagram. (a) Schematic diagram of 3D scanning; (b) composition diagram of 3D scanning system.

impact points. The 3D alignment process requires selecting several calibration points on the camera image and controlling the reflecting mirrors under camera guidance to sequentially direct laser beams from the three probes onto different points simultaneously. Therefore, establishing a mathematical model for light rays emitted from two cascaded rotating mirrors is necessary before obtaining the coordinates of calibration points in each PCS.

2.2. Solving of the rotation matrix

2.2.1. Establishment of a mathematical model of rotating mirror outgoing rays. To determine the rotation matrices that transform from the PCS to the WCS, mathematical model of light rays emitted from rotating mirrors must first be established. The 2D rotating mirror and laser beam reflection model utilized in this paper is illustrated in figure 2. In this model, mirrors M1 and M2 are controlled by two separate motors to rotate, with their rotation axes perpendicular to each other. The rotation angles of the mirrors exhibit a linear relationship with the input voltages of the motors. By adjusting the input voltages of each motor, mirrors M1 and M2 rotate accordingly, directing the laser beam to any desired point within the 3D scanning region.

The investigation begins by establishing a right-handed Cartesian coordinate system O_2-XYZ as the PCS, with the center point O_2 of mirror M2 as its origin and the Y-axis aligned with the rotation axis of mirror M2. Mirrors M1 and M2 have their rotation axis positions and initial angles fixed during manufacturing, with clockwise rotation defined as the positive direction for both mirrors. As illustrated in figure 2(b), the

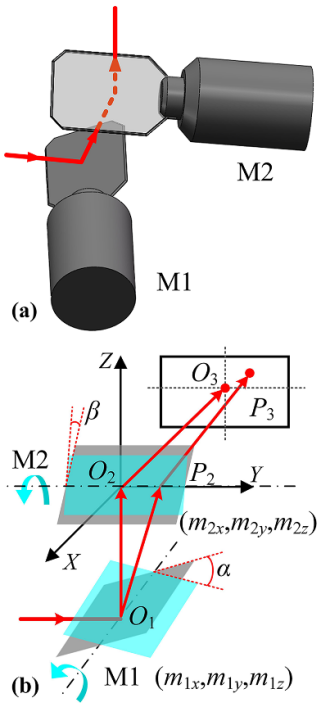

Figure 2. Laser rotation control model via two-axis rotating mirror. (a) Rotating mirror's geometric mode; (b) laser beam reflection model.

rotation angles of mirrors M1 and M2 relative to their initial angles are denoted as α and β, respectively, where the laser beam passes through the centers of M1 and M2 sequentially when $\alpha = \beta = 0$. In the O_2-*XYZ* coordinate system, the unit spatial vector of the incident laser beam is defined as $\mathbf{S} = (0,1,0)^{\mathrm{T}}$; the unit vectors of the rotation axes for mirrors M1 and M2 are represented as $\mathbf{m}_1 = (m_{1x}, m_{1y}, m_{1z})^{\mathrm{T}}$ and $\mathbf{m}_2 = (m_{2x}, m_{2y}, m_{2z})^{\mathrm{T}}$, respectively; and the initial normal vectors of M1 and M2 are expressed as $\mathbf{n}_1 = (n_{1x}, n_{1y}, n_{1z})^{\mathrm{T}}$ and $\mathbf{n}_2 = (n_{2x}, n_{2y}, n_{2z})^{\mathrm{T}}$.

The rotation matrix $\mathbf{R}_1$ of the normal vector of rotating mirror M1 was constructed using the unit vector $\mathbf{m_1}$ of the rotation axis of M1 [23],

$$\mathbf{R}_1 = e^{\widehat{\gamma}_1 \alpha} = \mathbf{I} + \widehat{\gamma}_1 \sin\alpha + \widehat{\gamma}_1^2 (1 - \cos\alpha) \tag{4}$$

where ***I*** represents the identity matrix, and

$$\widehat{\gamma}_1 = \begin{pmatrix} 0 & -m_{1z} & m_{1y} \\ m_{1z} & 0 & -m_{1x} \\ -m_{1y} & m_{1x} & 0 \end{pmatrix} . \tag{5}$$

The reflection matrix of M1 for the laser beam is defined as [24],

$$\mathbf{M}_1 = \left(\mathbf{I} - 2\left(\mathbf{R}_1\mathbf{n}_1\right)\left(\mathbf{R}_1\mathbf{n}_1\right)^{\mathrm{T}}\right) . \tag{6}$$

In the O_2-*XYZ* coordinate system, the coordinates of the center point O_1 of rotating mirror M1 are known, and the normal vector of M1 is defined as $\mathbf{n}_{1\alpha} = \mathbf{R}_1\mathbf{n}_1$. The unit vector of $\overrightarrow{\mathbf{O_1P_2}}$ can be obtained by left-multiplying the incident vector $\mathbf{S}$ with the mirror matrix $\mathbf{M}_1$. Therefore, O_1 and $\mathbf{n}_{1\alpha}$ uniquely determine the linear equation of the laser beam **O1P2** after reflection from M1. Similarly, the normal vector of M2 is expressed as $\mathbf{n}_{2\beta} = \mathbf{R}_2\mathbf{n}_2$, $\mathbf{O}_2 = (0,0,0)^{\mathrm{T}}$ and $\mathbf{n}_{2\beta}$ uniquely determines the plane equation of M2. Consequently, the intersection point P_2 of $\overrightarrow{\mathbf{O_1P_2}}$ and M2 can be calculated, which represents the reflection point of the laser beam on M2.

The reflection matrix of M2 for the laser beam is as follows,

$$\mathbf{M}_2 = \left(\mathbf{I} - 2\left(\mathbf{R}_2\mathbf{n}_2\right)\left(\mathbf{R}_2\mathbf{n}_2\right)^{\mathrm{T}}\right) . \tag{7}$$

Therefore, the unit vector of $\overrightarrow{\mathbf{P_2P_3}}$ after the laser beam's reflection from rotating mirrors M1 and M2 is expressed as:

$$\overrightarrow{\mathbf{P_2P_3}} = \mathbf{M}_2\mathbf{M}_1\mathbf{S} . \tag{8}$$

The position vector of the laser beam's impact point on the measured object can be determined by using the intersection vector $\overrightarrow{\mathbf{O_2P_2}}$, the unit vector $\overrightarrow{\mathbf{P_2P_3}}$ of the emitted laser beam, and the distance L between the emission point and the measured object,

$$\overrightarrow{\mathbf{O_2P_3}} = \overrightarrow{\mathbf{O_2P_2}} + L \cdot \overrightarrow{\mathbf{P_2P_3}} . \tag{9}$$

In the O_2-*XYZ* coordinate system of the 2D rotating mirror system designed in this study, the unit vectors of the rotation axes of M1 and M2 are $\mathbf{m_1} = (1,0,0)^{\mathrm{T}}$ and $\mathbf{m_2} = (0,1,0)^{\mathrm{T}}$, respectively. The coordinates of the center O_1 of M1 are $(0,0,-d)^{\mathrm{T}}$, where d represents the distance between the center points of rotating mirrors M1 and M2, determined by the geometric parameters of the fixed rotating mirror structure. The reference plane of rotating mirror M1 is defined as the XO_2Z plane, with its initial normal vector $\mathbf{n_1} = (0,-1,0)^{\mathrm{T}}$, while the reference plane of rotating mirror M2 is defined as the YO_2Z plane, with its initial normal vector $\mathbf{n_2} = (-1,0,0)^{\mathrm{T}}$. Typically, the initial planes of the 2D rotating mirrors form certain angles with their respective reference planes, where the angle between the initial position of rotating mirror M1 and the XO_2Z plane is defined as θ_x, and the angle between the initial position of rotating mirror M2 and the YO_2Z plane is defined as θ_y. Typically, the initial angles of the two rotating mirror axes are 45°. Based on the aforementioned derived formulas, the 3D coordinates of the emitted beam's unit vector $\overrightarrow{\mathbf{P_2P_3}} = (X,Y,Z)$ can be expressed as:

$$\begin{aligned} X = -4 &(\cos\alpha\sin\theta_x + \cos\theta_x\sin\alpha)\cdot \\ &(\cos\alpha\sin\theta_x - \sin\theta_x\sin\alpha)\cdot \\ &(\cos\beta\sin\theta_y + \cos\theta_y\sin\beta)\cdot \\ &(\cos\beta\sin\theta_y - \sin\theta_y\sin\beta) \end{aligned} \tag{10}$$

$$Y = 1 - 2(\cos\alpha\sin\theta_x - \cos\theta_x\sin\alpha)^2 \tag{11}$$

$$Z = -2\left(\cos\alpha\sin\theta_x + \cos\theta_x\sin\alpha\right)\cdot \left(\cos\alpha\cos\theta_x - \sin\theta_x\sin\alpha\right)\cdot \left(2\cos\beta\sin\theta_y + 2\cos\theta_y\sin\beta - 1\right). \tag{12}$$

In the 2D rotating mirror system employed in this study, the vector $\overrightarrow{\mathbf{O_2P_2}}$ of the beam emission point on rotating mirror M2 is expressed as:

$$\overrightarrow{\mathbf{O_2P_2}} = \left(0, -d\cdot\tan\left(2\alpha\right), 0\right)^{\mathrm{T}}. \tag{13}$$

By combining equations (9) through (13), the spatial coordinates of the laser beam impact point in the PCS can be determined as,

$$X = -4L\left(\cos\alpha\sin\theta_x + \cos\theta_x\sin\alpha\right)\cdot \left(\cos\alpha\sin\theta_x - \sin\theta_x\sin\alpha\right)\cdot \left(\cos\beta\sin\theta_y + \cos\theta_y\sin\beta\right)\cdot \left(\cos\beta\sin\theta_y - \sin\theta_y\sin\beta\right) \tag{14}$$

$$Y = L\cdot\left[1 - 2\left(\cos\alpha\sin\theta_x - \cos\theta_x\sin\alpha\right)^2\right] - d\cdot\tan\left(2\alpha\right) \tag{15}$$

$$Z = -2L\left(\cos\alpha\sin\theta_x + \cos\theta_x\sin\alpha\right)\cdot \left(\cos\alpha\cos\theta_x - \sin\theta_x\sin\alpha\right)\cdot \left(2\cos\beta\sin\theta_y + 2\cos\theta_y\sin\beta - 1\right) \tag{16}$$

where θ_x and θ_y are determined by the mechanical structure of the rotating mirror system, and L represents the distance between the emission point O_2 of the rotating mirror and the impact point on the structure to be measured, which can be calculated using the following equation:

$$L = D - D_1 \tag{17}$$

where D represents the distance measured by the laser rangefinder, and D_1 denotes the fixed distance from the vibrometer laser emission point to the output point of the rotating mirror system, which is determined by the mechanical assembly.

2.2.2. 3D alignment algorithm. The alignment method proposed in this paper directly establishes the WCS on the measured object. During the process of establishing the WCS, rotation matrices between each PCS and the WCS are constructed, enabling 3D vibration analysis without relying on external calibration tools, avoiding positioning errors of calibration plates and environmental interference effects in traditional methods, and directly correlating with the measured object surface. Therefore, this method can intuitively measure 3D vibration vectors on the measured object surface while ensuring the orthogonality and physical significance of the transformation matrices.

The coordinate system established in this paper is illustrated in figure 3. During the establishment of the coordinate system, a point A is arbitrarily selected on the surface of the measured object as the origin of the WCS, and the calibrated rotating mirror system converges the emitted laser beams from three probes onto point A. The spatial vectors of point A in the three PCSes, denoted as $\overrightarrow{\mathbf{T_1A_1}}$, $\overrightarrow{\mathbf{T_2A_2}}$, and $\overrightarrow{\mathbf{T_3A_3}}$, are derived from equations (14) through (16), where T1, T2, and T3 represent the emission points of the laser beams from the three probes, respectively. Using the same method, points B and C are selected, resulting in the vectors $\overrightarrow{\mathbf{T_1B_1}}$, $\overrightarrow{\mathbf{T_2B_2}}$, $\overrightarrow{\mathbf{T_3B_3}}$ and $\overrightarrow{\mathbf{T_1C_1}}$, $\overrightarrow{\mathbf{T_2C_2}}$, and $\overrightarrow{\mathbf{T_3C_3}}$.

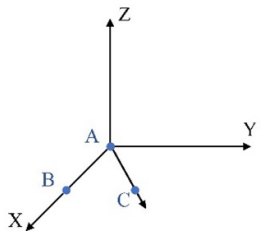

Figure 3. Schematic diagram for directly establishing the WCS.

As illustrated in figure 3, the vector $\overrightarrow{\mathbf{AB}}$ is defined as the X-axis of the WCS, with the plane determined by points A, B, and C established as the XY plane, and the normal vector of this plane designated as the direction of the Z-axis of the coordinate system. Taking the spatial vectors $\overrightarrow{\mathbf{T_1A_1}}$, $\overrightarrow{\mathbf{T_1B_1}}$, and $\overrightarrow{\mathbf{T_1C_1}}$ in one PCS as an example, the unit vector in the X-axis direction can be derived as,

$$\mathbf{x}' = \frac{\overrightarrow{\mathbf{T_1B_1}} - \overrightarrow{\mathbf{T_1A_1}}}{\left|\overrightarrow{\mathbf{T_1B_1}} - \overrightarrow{\mathbf{T_1A_1}}\right|}. \tag{18}$$

Consequently, the unit vectors in the Z-axis and Y-axis directions are expressed as,

$$\mathbf{z}' = \frac{\overrightarrow{\mathbf{T_1C_1}} - \overrightarrow{\mathbf{T_1A_1}}}{\left|\overrightarrow{\mathbf{T_1C_1}} - \overrightarrow{\mathbf{T_1A_1}}\right|} \tag{19}$$

$$\mathbf{y}' = \mathbf{z}' \times \mathbf{x}' \tag{20}$$

where $\mathbf{x}'$, $\mathbf{y}'$, and $\mathbf{z}'$ are all 3×1 unit vectors. Based on these vectors, the rotation matrix $\mathbf{R}_1$ between the PCS and the WCS can be constructed as,

$$\mathbf{R}_1 = \begin{bmatrix} \mathbf{x}'^{\mathrm{T}} \\ \mathbf{y}'^{\mathrm{T}} \\ \mathbf{z}'^{\mathrm{T}} \end{bmatrix} = \begin{bmatrix} \mathbf{x}'_x & \mathbf{x}'_y & \mathbf{x}'_z \\ \mathbf{y}'_x & \mathbf{y}'_y & \mathbf{y}'_z \\ \mathbf{z}'_x & \mathbf{z}'_y & \mathbf{z}'_z \end{bmatrix}. \tag{21}$$

Similarly, the rotation matrices $\mathbf{R}_2$ and $\mathbf{R}_3$ between the other two PCSes and the WCS can be constructed, thereby enabling the measurement of 3D vibration in the orthogonal WCS through equation (3) via substituting the non-orthogonal vibration velocity components measured by the three probes along their respective laser beam directions.

2.3. Experiments

To evaluate the precision of the alignment method proposed in this paper, an aluminum plate with dimensions of 400 mm × 300 mm × 3 mm was selected as the test object to

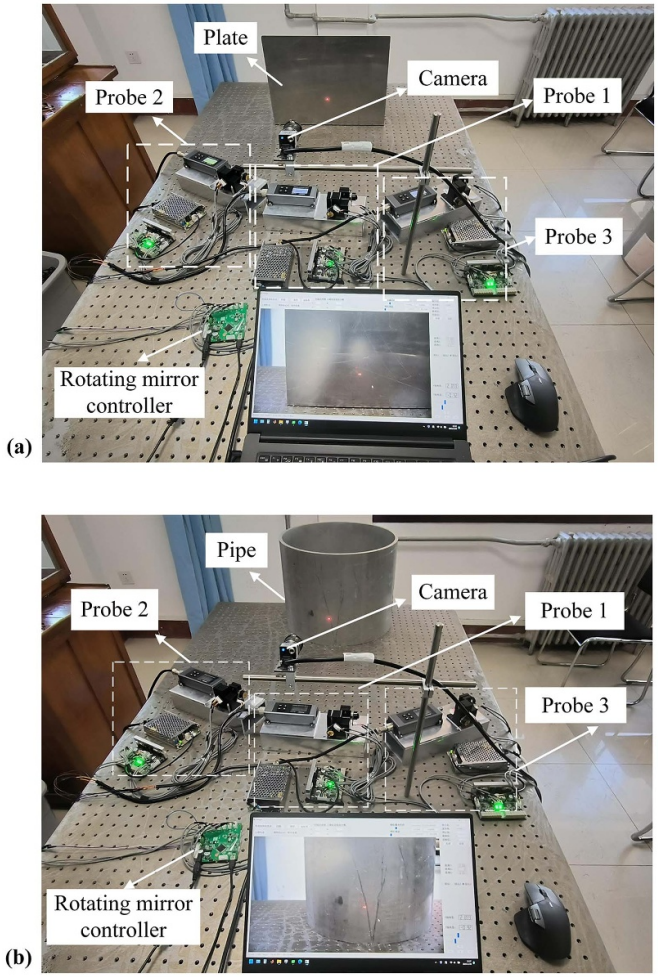

Figure 4. Experimental system. (a) Plate alignment experiment; (b) pipe alignment experiment.

simulate common structural surfaces, while a cylindrical pipe with a diameter of 400 mm, height of 300 mm, and wall thickness of 10 mm was chosen as a representative curved surface object. The experimental system was constructed as illustrated in figure 4.

The experimental system consists of three identical laser probes and one camera, with each probe equipped with a laser rangefinder and a 2D rotating mirror system. Through mechanical design and optical path adjustment, the laser emitted from the rangefinder is ensured to precisely incident on the geometric center of the rotating mirror M1.

3. Results and discussion

3.1. Error assessment methods

Currently, most existing studies adopt coordinate-based methods for rotation matrix error evaluation, which involve setting several test points on the measured object and calculating errors through their coordinates. However, this approach only calculates errors based on limited test points, failing to comprehensively assess algorithm performance across the entire scanning space or reflect systematic errors from laser beam directional variations. To address these limitations, this paper proposes and adopts an error evaluation method based on the expression of laser beam unit direction vectors in spherical coordinate system. Considering the practical requirement that laser beams need to cover the entire workspace in scanning measurement, this method can comprehensively assess alignment algorithm performance across the entire laser scanning range, providing a more accurate and complete evaluation of system performance.

The expression of any detection laser's unit vector in space under the spherical coordinate system is defined as,

$$\mathbf{L} = (\sin\alpha\cos\beta, \sin\alpha\sin\beta, \cos\alpha)^{\mathrm{T}} \tag{22}$$

where α represents the angle between the vector and the Z-axis of the PCS, with $\alpha \in (0, \pi)$; and β denotes the angle between the projection of the vector on the XOY plane and the X-axis, and $\beta \in (0, \pi)$. Based on the relative pose relationship of the vibrometer probes during placement, the reference rotation matrix $\mathbf{R_c}$ can be calculated, which subsequently enables the determination of the corresponding unit vectors $\mathbf{L_w}$ and $\mathbf{L_{wc}}$ in the WCS,

$$\begin{cases} \mathbf{L_w} = \mathbf{RL} \\ \mathbf{L_{wc}} = \mathbf{R_c L} \end{cases}. \tag{23}$$

The error vector $\mathbf{E}$ is obtained by subtracting the reference result $\mathbf{L_{wc}}$ from the calculated result $\mathbf{L_w}$,

$$\mathbf{E} = \mathbf{L_w} - \mathbf{L_{wc}} = (E_x, E_y, E_z) \tag{24}$$

where E_x, E_y, and E_z represent the X-axis, Y-axis, and Z-axis components of the error vector $\mathbf{E}$, respectively. According to equation (21), the velocity vectors in the PCSes are transformed by rotation matrices to the WCS and then superimposed to generate 3D vibrometry data. Therefore, the error vector $\mathbf{E}$ directly represents the measurement result errors introduced by the rotation matrices.

Finally, the L2-norm of the error vector $\mathbf{E}$ is double-integrated over the domains of α and β to obtain E_{err} as the overall error assessment variable,

$$E_{\mathrm{err}} = \frac{\int_0^{\pi}\int_0^{\pi} \|\mathbf{E}\|_2 \mathrm{d}\beta\mathrm{d}\alpha}{\pi^2}. \tag{25}$$

In this study, the error vector $\mathbf{E}$ is defined as the difference between two unit vectors. When the two unit vectors are aligned in the same direction, the L2-norm equals 0; when they are in opposite directions, the L2-norm equals 2. The average error E_{err} is a dimensionless quantity with a range of 0–2, characterizing the degree of directional deviation between vectors. This evaluation method directly represents the measurement errors along the three axes caused by errors in the rotation matrices, while also providing an overall error assessment through double integration as an evaluation criterion. Compared to traditional evaluation methods based on limited test points, this method can reflect potential errors of laser beams in arbitrary directions throughout the entire scanning space, providing more comprehensive quantitative

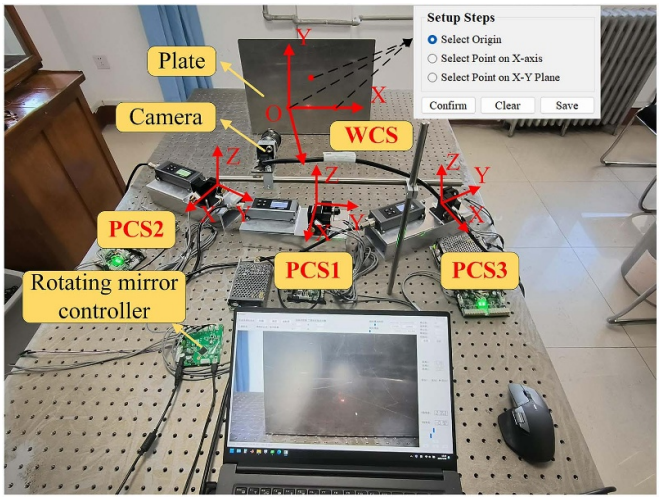

Figure 5. Schematic diagram of the coordinate system for the plate alignment experiment.

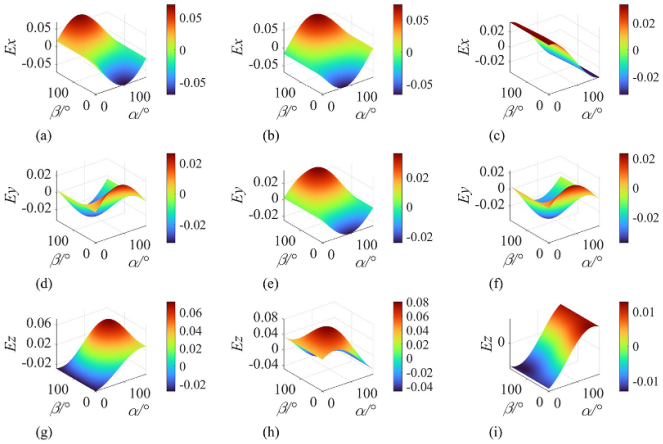

Figure 6. Plate alignment experiment error. (a)–(c) Error of the probes 1, 2, 3 in the X direction; (d)–(f) error of the probes 1, 2, 3 in the Y direction; (d)–(f) error of the probes 1, 2, 3 in the Z direction.

assessment of algorithm performance, and is particularly suitable for industrial vibration measurement applications requiring FFS.

3.2. Plate alignment experiment

As illustrated in figure 5, the WCS was established on the plate, with the plate surface serving as the *XOY* plane of the WCS and the Z-axis of the WCS perpendicular to the plate. The *YOZ* plane of the probe 1 is parallel to the *XOY* plane of the WCS.

According to the definitions related to coordinate system rotation transformations, when the coordinate system rotates around the X-axis, its rotation matrix $\mathbf{R_x}$ is expressed as,

$$\mathbf{R_x} = \begin{bmatrix} 1 & 0 & 0 \\ 0 & \cos\theta_1 & -\sin\theta_1 \\ 0 & \sin\theta_1 & \cos\theta_1 \end{bmatrix} \tag{26}$$

where θ_1 represents the rotation angle around the X-axis. Similarly, when the coordinate system rotates around the Y-axis and Z-axis, the rotation matrices $\mathbf{R_y}$ and $\mathbf{R_z}$ are expressed as follows, respectively,

$$\mathbf{R_y} = \begin{bmatrix} \cos\theta_2 & 0 & \sin\theta_2 \\ 0 & 1 & 0 \\ -\sin\theta_2 & 0 & \cos\theta_2 \end{bmatrix} \tag{27}$$

$$\mathbf{R_z} = \begin{bmatrix} \cos\theta_3 & -\sin\theta_3 & 0 \\ \sin\theta_3 & \cos\theta_3 & 0 \\ 0 & 0 & 1 \end{bmatrix} \tag{28}$$

where θ_2 and θ_3 represent the rotation angles of the coordinate system around the Y-axis and Z-axis, respectively.

Based on the established coordinate systems described above, the reference rotation matrix $\mathbf{R}_{c1}^{\mathbf{Plate}}$ between the PCS1 and the WCS can be determined as,

$$\mathbf{R}_{c1}^{\mathbf{Plate}} = \mathbf{R_x} \cdot \mathbf{R_z} = \begin{bmatrix} 0 & 1 & 0 \\ 0 & 0 & 1 \\ 1 & 0 & 0 \end{bmatrix}. \tag{29}$$

In the experiment, probe 2 and probe 3 were rotated clockwise around the Z-axis by $-22°$ and $20°$, respectively, relative to the probe 1. Calculations determine that the reference rotation matrices $\mathbf{R}_{c2}^{\mathbf{Plate}}$ and $\mathbf{R}_{c3}^{\mathbf{Plate}}$ between the remaining probes and the WCS are expressed as, respectively,

$$\mathbf{R}_{c2}^{\mathbf{Plate}} = \begin{bmatrix} 0.375 & 0.927 & 0 \\ 0 & 0 & 1 \\ 0.927 & -0.375 & 0 \end{bmatrix} \tag{30}$$

$$\mathbf{R}_{c3}^{\mathbf{Plate}} = \begin{bmatrix} -0.342 & 0.940 & 0 \\ 0 & 0 & 1 \\ 0.940 & 0.342 & 0 \end{bmatrix}. \tag{31}$$

The results of the 3D alignment experiment in the plate scenario are illustrated in figure 6.

As observed in figure 6, for emission vectors at arbitrary angles, the errors of the three vibrometer probes in all three axial directions are less than 8%. The L2-norm of the error vector under different alignment point distributions is calculated using equation (25), followed by double integration over the domains of α and β, yielding average errors of 5.18% for the probe 1, 5.69% for probe 2, and 3.07% for probe 3. The average relative errors of all three probes are below 2.85%, validating the accuracy of the alignment algorithm when applied to plate scenarios.

3.3. Pipe alignment experiment

As illustrated in figure 7, the WCS in the 3D alignment experiment is established on the pipe, with the *XOY* plane of the WCS defined as the tangential plane of the pipe, and with the *YOZ* plane of the probe 1 parallel to the *XOY* plane of the WCS.

Based on the established coordinate systems described above, the reference rotation matrix $\mathbf{R}_{c1}^{\mathbf{Pipe}}$ between the PCS 1 and the WCS can be determined as,

$$\mathbf{R}_{c1}^{\mathbf{Pipe}} = \mathbf{R_x} \cdot \mathbf{R_z} = \begin{bmatrix} 0 & 1 & 0 \\ 0 & 0 & 1 \\ 1 & 0 & 0 \end{bmatrix}. \tag{32}$$

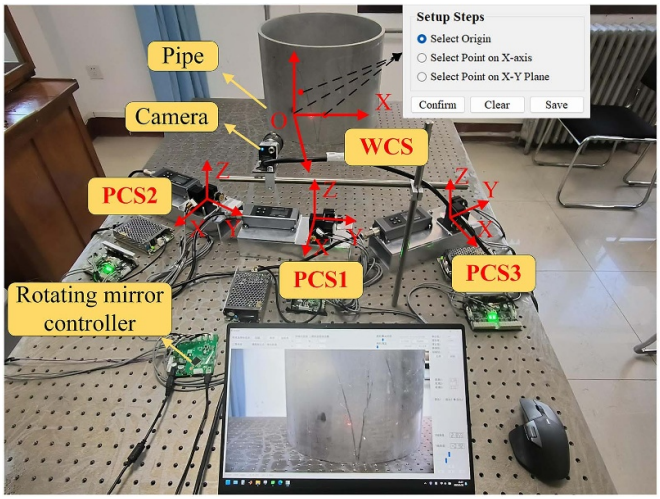

Figure 7. Schematic diagram of the coordinate system for the pipe alignment experiment.

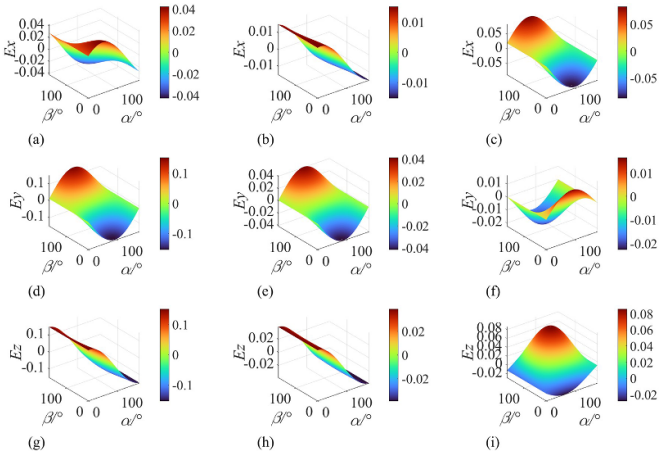

Figure 8. Pipe alignment experiment error. (a)–(c) Error of the probes 1, 2, 3 in the *X* direction; (d)–(f) error of the probes 1, 2, 3 in the *Y* direction; (d)–(f) error of the probes 1, 2, 3 in the *Z* direction.

In the experiment, the probes 2 and 3 were rotated clockwise around the *Z*-axis by $-13°$ and $20°$, respectively, relative to the probe 1. Calculations determine that the reference rotation matrices $\mathbf{R}_{c2}^{Pipe}$ and $\mathbf{R}_{c3}^{Pipe}$ between the remaining probes and the WCS are expressed as follows, respectively,

$$\mathbf{R}_{c2}^{Pipe} = \begin{bmatrix} 0.225 & 0.974 & 0 \\ 0 & 0 & 1 \\ 0.974 & -0.225 & 0 \end{bmatrix} \tag{33}$$

$$\mathbf{R}_{c3}^{Pipe} = \begin{bmatrix} -0.342 & 0.940 & 0 \\ 0 & 0 & 1 \\ 0.940 & 0.342 & 0 \end{bmatrix}. \tag{34}$$

As observed in figure 8, for laser beam emission vectors ranging from 0° to 180°, the three-axis alignment errors of all three probes are less than 15%. The probe 1 exhibits higher errors in the *Y*-axis and *Z*-axis directions (average error of 13.05%), and this is because there is slight angular deviations between its *YOZ* plane and the *XOY* plane that leads to imprecisions in the rotation matrix $\mathbf{R}_{c1}$. The average alignment error E_{err} is calculated using equation (25), and the yielding value is 13.05% for the probe 1, 3.5% for probe 2, and 5.83% for probe 3, with relative errors all below 6.53%. These experiment results validate that the alignment algorithm maintains good performance when applied to curved surface scenarios.

4. Conclusion

To address bottleneck issues in 3D FFS LDV, including the absence of laser beam emission models, insufficient multi-probe collaborative alignment precision, and low calibration efficiency on complex surfaces, this paper proposes a 3D alignment algorithm that directly establishes the WCS on the surface of the measured object based on a cascaded rotating mirror mathematical model. Additionally, we introduce a spherical coordinate-based double integral error evaluation method to overcome the limitations of traditional evaluation approaches that only assess local errors at limited test points, providing comprehensive performance assessment across the entire laser scanning range.

Building upon the established geometric model of laser beam emission from the 2D rotating mirrors, the 3D alignment algorithm is developed and validated using plate and pipe as representative targets to verify its effectiveness. Experimental validation demonstrated that the proposed algorithm achieves maximum average relative errors of 2.85% in plate measurement scenarios and 6.53% in curved surface measurement scenarios, meeting the engineering precision requirements for 3D vibration vector decomposition.

In conclusion, the method proposed in this study eliminates the need for auxiliary means such as calibration plates and theodolites, significantly enhancing the reliability and applicability of orthogonal 3D vibration measurements in the WCS on complex structures, thereby providing a high-precision, low-complexity systematic solution for industrial intelligent inspection scenarios. However, this method still has certain limitations: it has currently only been verified on relatively simple geometric structures, the selection of reference points is subjective, and it has certain requirements for the reflection characteristics of the measured surface. Future work needs to further verify the robustness and applicability of this method on more complex geometric structures, different surface characteristics, and actual engineering environments.

Data availability statement

All data that support the findings of this study are included within the article (and any supplementary files).

Acknowledgments

This work is supported by National Natural Science Foundation of China (No. 62473279), Natural Science Foundation of Tianjin (No. 24JCZDJC01070), and Guangxi

Key Laboratory of Automatic Detecting Technology and Instruments (No. YQ24203).

ORCID iDs

Huang Xinjing 0000-0002-8964-8502
Lai Ruqiang 0009-0001-0918-7102
Li Zhengzhe 0000-0003-0571-6318
Ma Jinyu 0000-0003-1509-9421

References

[1] Schewe M, Ismail M A A and Rembe C 2021 Towards airborne laser Doppler vibrometry for structural health monitoring of large and curved structures *Insight, Non-Destr. Test. Cond. Monit.* **63** 280–2
[2] Li L and Formme P 2024 Experimental validation of guided wave mode-conversion at part-thickness defects in metal plates *Proc. SPIE* **12951** 225–30
[3] Delo G *et al* 2024 Using the inverse finite-element method to harmonise classical modal analysis with fibre-optic strain data for robust population-based structural health monitoring *Strain* **61** e12481
[4] Yu Z Y, Tang Q X and Vinayaka S 2024 Identifying structural properties of a steel railway bridge for structural health monitoring using laser Doppler vibrometry *Autom. Constr.* **160** 105320
[5] Zhang L, Zang C and Jing T 2024 An adaptive continuous scanning laser Doppler vibrometry technique for measuring vibrational mode shapes of structures with holes *Meas. Sci. Technol.* **35** 115203
[6] Jin Y, Dollevoet R and Li Z 2022 Removing speckle noise from the signals of a laser Doppler vibrometer on moving platforms (LDVom) by ensemble empirical mode decomposition *Meas. Sci. Technol.* **33** 125205
[7] Hasheminejad N, Vuye C and Margaritis A 2019 Characterizing the complex modulus of asphalt concrete using a scanning laser Doppler vibrometer *Materials* **12** 1–18
[8] Hu Y H, Zhu W D, Yu K P, Yang Y and Kang Y 2025 Operational modal analysis of outdoor slanted rotational blades under natural excitation using a long-range tracking continuously scanning laser Doppler vibrometer *Opt. Laser Technol.* **181** 111516
[9] Kim D, Song H, Khalil H, Lee J, Wang S and Park K 2014 3-D vibration measurement using a single laser scanning vibrometer by moving to three different locations *IEEE Trans. Instrum. Meas.* **63** 2028–33
[10] Kim D and Park K 2013 Development of a three-dimensional vibration measurement system using a single laser scanning vibrometer and laser scanner *Int. Conf. on Control, Automation and Systems* (*Gwangju*) (IEEE) pp 1378–80
[11] Margerit P, Gobin T, Lebee A and Caron J-F 2021 The robotized laser Doppler vibrometer: on the use of an industrial robot arm to perform 3D full-field velocity measurements *Opt. Lasers Eng.* **137** 106363
[12] Sels S, Ribbens B, Bogaerts B, Peeters J and Vanlanduit S 2017 3D model assisted fully automated scanning laser Doppler vibrometer measurements *Opt. Lasers Eng.* **99** 23–30
[13] Sels S, Vanlanduit S, Bogaerts B and Penne R 2019 Three-dimensional full-field vibration measurements using a handheld single-point laser Doppler vibrometer *Mech. Syst. Signal Process.* **126** 427–39
[14] Huang Y, Zhao S, Chen M, Zhang D, Zhou Y and Shu X 2020 A non-contact dynamic attitude measurement system based on 3D oblique laser Doppler vibrometers *Proc. SPIE* **11567** 379–84
[15] Rembe C, Kowarsch R, Ochs W, Dräbenstedt A, Giesen M and Winter M 2014 Optical three-dimensional vibrometer microscope with picometer-resolution in x, y, and z *Opt. Eng.* **53** 34108
[16] Miyashita T and Fujino Y 2006 Development of 3D vibration measurement system using laser Doppler vibrometers *Proc. SPIE - Int. Soc. Opt. Eng.* **6177** 170–9
[17] Chen D and Zhu W D 2017 Investigation of three-dimensional vibration measurement by a single scanning laser Doppler vibrometer *J. Sound Vib.* **387** 36–52
[18] Yuan K and Zhu W D 2023 Identification of modal parameters of a model turbine blade with a curved surface under random excitation with a three-dimensional continuously scanning laser Doppler vibrometer system *Measurement* **214** 112759
[19] Song Y *et al* 2018 Research on three-dimensional scanning vibrometry based on laser Doppler technology *Mech. Eng.* 150152+159 (available at: https://kns.cnki.net/kcms2/article/abstract?v=GWCpWhBv_VNcMBPtS2xUk8GrlpQKcNThQLtgIgEzkTUu2AAKWNDN6gGSSfZnA69Dd8EcuQrPwvoR3Dg4IffaSqijVlDv2JzMZghmOXcoDa94AbHFYFIFwsiS_yQFIz93KIlJFryYA7TdAyTAJHygf5eWJ4voojfYvqZJ6yuRX-E=&uniplatform=NZKPT)
[20] Zeng X D, Wicks A L and Mitchell L D 1996 Geometrical method for the determination of the position and orientation of a scanning laser Doppler vibrometer *Opt. Lasers Eng.* **25** 247–64
[21] Martarelli M, Revel G M and Santolini C 2001 Automated modal analysis by scanning laser vibrometry: problems and uncertainties associated with the scanning system calibration *Mech. Syst. Signal Process.* **15** 581–601
[22] Xu Y C and Miles R N 1995 An identification algorithm for directing the measurement point of scanning laser vibrometers *Opt. Lasers Eng.* **22** 105–20
[23] Huang X J, Chen S L, Guo S X, Xu T, Ma Q, Jin S and Chirikjian G S 2017 A 3D localization approach for subsea pipelines using a spherical detector *IEEE Sens. J.* **17** 1828–36
[24] Jia G, Hou L and Hong P 2021 Research on model of image rotation of reflective two-dimensional fast-steering mirror *Opt. Optoelectron. Technol.* **19** 86–92 (available at: https://kns.cnki.net/kcms2/article/abstract?v=GWCpWhBv_VM6l45FaDhY2gYjrIwed-hrtYoZQ-BZe3XSD0AgldzZfAD2PHyISzYtWQhyFibqnp0vYNHm-3DoXPaqIlpoltz1OQZHdq40Xn-EOw0RDkcx29-IQ3MiGIISPnmf-JGx-e4fqa50iJnYV4u2yj_2t7mRqMHsyHkcEUI=&uniplatform=NZKPT)